Infrared spectroelectrochemical configurations for *in situ* measurements

NEBOJŠA S. MARINKOVIĆ[1]* and RADOSLAV R. ADŽIĆ[2]

[1]*Synchrotron Catalysis Consortium and Department of Chemical Engineering, Columbia University, New York, NY 10027, USA and* [2]*Department of Chemistry, Brookhaven National Laboratory, Upton, NY 11973, USA*

Abstract: The choice of infrared (IR) spectroelectrochemical configurations and accessories depends on the type of reaction investigated. The mostly used system is Otto configuration where the electrolyte is squeezed between the electrode and the internal reflection element (IRE). However, another system with the film electrode deposited directly onto the flat side of the IRE (Kretschmann configuration) gains popularity, not only because of the increase in sensitivity, but also as it allows electrochemical reactions involving gas evolution. By the use of Fresnel equations for three-phase stratified medium we show that the strength of mean-square electric field (MSEF) at the metal/solution interface, associated with the dissipation of energy onto the adsorbed species in Otto configuration, is rather flexible in the choice of the optimal angle of incidence of the IR radiation and the thickness of the water layer. On the other hand, Kretschmann configuration is very sensitive to the parameters of the optical system, so the calculations of the MSEF are necessary to identify the optimal angle of incidence and the thickness of the metal layer that give maximal enhancement in the mid-IR region where the bands of interest occur.

Keywords: Kretschmann configuration; Otto configuration; IRRAS; electric field; Fresnel equations.

INTRODUCTION

Since the pioneering works in Infrared spectroscopy and the development of Fourier transform infrared spectroscopy (FTIR), it became obvious that a number of materials cannot be investigated by the simple transmission method. A variety of techniques including attachments for specular reflection, reflection-absorption, attenuated total reflection and diffuse reflectance spectrometry were developed for investigation of a flat surface of thick and thin absorbing material, liquids and powders.[1,2] These attachments were essential in analysis of various surfaces,

---

*Corresponding author. E-mail: marinkov@bnl.gov

including corrosion products and inhibitors, as well as in the analysis of the growth of metal protective layers and film thickness, giving insights in both organic and inorganic chemical reactions. In electrochemistry, a special attachment was developed for the study of species adsorbed on metal/electrolyte interface.

Following the pioneering work on IR reflectance spectroscopy at metal surfaces,[3–6] the application to studying electrode/electrolyte interface was described in the sixties.[7–10] The most common configuration (termed Otto configuration) for internal infrared (IR) spectroelectrochemistry consists of internal reflection element (IRE), solution and the metal electrode in which the IR beam traverses through the infrared-transparent IRE (prism or hemisphere) of a high refractive index and totally reflects from the IRE/solution interface.[11, 12] Simultaneously, an evanescent wave develops at the interface and propagates further into the rarer medium (solution). If the electrode surface is positioned within the reach of the penetration depth of the evanescent wave (1–3 μm), the reflected beam traveling to the IR detector is attenuated and carries the absorption of species in the electrolyte and at the metal surface. If the metal surface serves as the working electrode in an electrochemical setup, the difference in the electrode potential induces the rearrangement of species in the electrochemical double layer and can be monitored by the technique. The reflected beam, R_0, at the potential, E_0, which is outside of the potential region in which the studied electrochemical reaction takes place, contains the information of the solution species only and can serve as the reference signal. At the potential where the reaction takes place, E_1, the species in the solution layer and those adsorbed on the electrode surface rearrange so that the reflected IR beam (R_1) contains the information on them. By subtracting the reflected IR signals at the two potentials and scaling to unity by dividing the difference with the reflected beam at E_0, the resulting spectrum $-\Delta R/R = (R_1 - R_0)/R_0$ contains both positive and negative peaks arising from accumulation and depletion of species in the optical path, respectively. It can be shown that this subtractively normalized signal ($-\Delta R/R$) is proportional to absorbance.[13]

Otto configuration is applicable to most electrode surfaces including smooth polycrystalline and single crystal surfaces, as well as on the powdered catalysts embedded into a conductive medium (*e.g.*, carbon) and attached onto an electrode of inactive material (*e.g.*, gold).[11,13] A great volume of literature deals with the Otto configuration and its applications to electrochemistry.[14–17] On the other hand, considerably less work in spectroelectrochemistry uses another configuration in which the solution and the working electrode are interchanged. In this setup, the working electrode is in the form of a thin metal film deposited directly on the flat surface of the IRE element and the solution layer is semi-infinite, thus allowing gaseous products to escape (Fig. 1). In addition, the later configuration that is usually referred to as Kretschmann configuration is a powerful tool for adsorbates at the metal surface because high-absorbing effects of the solution

layer are avoided.[18] As shown further, the electric field strength (EFS) that probes the metal/solution interface can be orders of magnitude higher than that of the Otto configuration.[19] Unfortunately, Kretschmann configuration is applicable only to a limited number of electrodes consisting of metal layers that can be deposited onto the IRE in a film of a thickness of a few tens of nm. Consequently, studies involving single crystal surfaces and powdered catalysts are difficult.

The sensitivity of both configurations depends strongly on the incidence angle at the metal/solution interface. In the present paper, we discuss the optimization of both configurations, based on the theoretical calculations of the electric field strength and show that a slight misalignment can result in the several times lower sensitivity.

RESULTS AND DISCUSSION

Calculation of the electrical field in this work is based on the equations developed by Hansen.[20,21] The difference in the formulas in the two works arises from the choice of the sign of the imaginary term in the complex index of refraction $\tilde{n}$. In this work, the positive sign ($\tilde{n} = n + i\kappa$) is used, as in the later work by Hansen.[21] These equations can be inserted into a number of mathematical programs that support complex number calculations (*e.g.*, MathLab or Mathematica) and/or certain widely used programs (Microsoft Excel), as well as web-based programs (Wolfram Alpha).[22]

Electric field and reflectivity calculations

For the calculations presented below, we used the three-layer system comprised of zinc selenide, platinum and water phases, where the thicknesses of the first and third phases are assumed infinite, and the thickness of the second layer is h in the direction of propagation of the IR light. The optical constants for ZnSe, platinum and water are available in the literature.[23] The optical constant for dilute aqueous solutions is assumed to be close to that of water. The difference in the calculations below is in the placement of the solution layer and is explicitly specified.

When an electromagnetic radiation passes from one phase into the next, its speed and strength depend on the indices of refraction of the two phases. The index of refraction is usually expressed as a complex number, $\tilde{n} = n + i\kappa$, consisting of the real part n expressed as the ratio of the speed of light in vacuum relative to that in the phase ($n = c/v$), and the extinction coefficient κ that is related to the attenuation of the light in that phase. For optically transparent phases, the extinction coefficient is zero, and for absorbing phases where $\kappa > 0$, the light is attenuated by the medium and its electric field exponentially decays, as expected by Beer's law. The penetration depth, or the distance at which the electric field decays to $1/e$, depends on the extinction coefficient as $d_p = \lambda_0/4\pi\kappa$, where λ_0 is the wavelength of the radiation in vacuum.

The refraction of light for two-phase system is described by Snell's Law, which is in the general form:[21]

$$n_1 \sin\theta_1 = \tilde{n}_i \sin\theta_i \qquad (1)$$

where phase i is any phase in the stratified medium, the phase 1 is assumed optically transparent so that $\tilde{n}_1 = n_1$ and θ_1 is real, and the angles θ_1 and θ_i (which is generally complex) are measured towards the surface normal. In the case of the light propagating from an optically denser into optically rarer medium ($n_1 > n_2$) of a two-phase system (Fig. 1a), there exists a critical angle $\theta_c = \sin^{-1}(n_2/n_1)$ at which the beam is refracted parallel to the interface of the two phases, *i.e.*, $\theta_2 = 90°$ and $\sin\theta_2 = 1$. At incidence angles larger than θ_c, θ_2 becomes imaginary and the refracted beam is reflected into the denser medium, but carries the information on the absorption of species in the rarer medium. This phenomenon applies even if the phase 2 is absorbing, as long as $\kappa_2 \ll 1$ and is utilized in infrared spectroelectrochemistry in aqueous solutions, as the extinction coefficient for water in most of mid-IR range (4000–1000 cm^{-1}) spans from 0.01 to 0.06 even around OH--bending mode (~1600 cm^{-1}).[23]
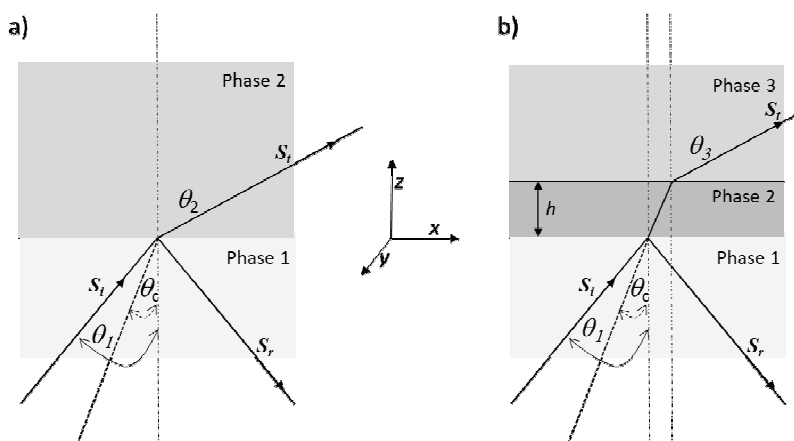

Fig. 1. Two- (a) and three-phase optical system (b). The incident beam given by Poynting vectors S_i strikes the phase 1/phase 2 interface at the angle θ that is greater than the critical angle θ_c and splits into reflected and transmitted portions S_r and S_t. The second phase of the three-phase system has the thickness h.

In a three-phase system the direction of the refracted light depends only on the refractive indices of the initial and the final phase, as the optical properties and the thickness of the phase 2 affect only the magnitude of the Poynting vector of the transmitted light (Fig. 1b). If the thickness of the 2nd layer is small ($h < \lambda$) in comparison to the wavelength of the incident radiation, there also exists a critical angle at which the total refraction occurs, $\theta_c = \sin^{-1}(n_3/n_1)$, and the evanescent wave is generated for $\theta > \theta_c$ when the extinction coefficients are $\kappa_3 \ll 1$. This

phenomenon is used in Kretschmann configuration. Therefore, it is not surprising that the same optical arrangement setup can be used for both Otto and Kretschmann configurations.

The optical properties of a phase can be completely characterized using the (dimensionless) magnetic permeability relative to free space μ and the complex index of refraction. Because most materials, including water and Pt, have magnetic permeability very close to unity,[24] the exact formulas given in Hansen[20,21] can be somewhat simplified.

At the interface of any two phases, the polarization state of both reflected and transmitted lights change. These effects are treated by Fresnel equations separately for the two components of the light, *i.e.*, the component polarized parallel to the plane containing the incident, reflected and refracted rays (*p*-polarized light or transverse-magnetic), and the component perpendicular to the above plane (*s*-polarized light or transverse-electric). The absorption of a phase is given as the energy dissipated in the unit volume of the phase per unit time and is defined as the product of conductivity σ and the mean square electric field (MSEF), $<E_z^2>$. The conductivity $\sigma = n\kappa\nu/\mu$ is related to the optical properties of the absorbing phase and the frequency of the light ν, whereas the magnitude of MSEF depends on the refractive indices of all media in the light's path, as well as on thickness of the second layer and the angle of incidence of the radiation into the first medium θ_1. All optical constants are assumed independent on the electrode potential. Because of the surface selection rule,[13] the light induces vibrations of molecules that have dipole moment perpendicular to the surface (or parallel to the plane containing incident and transmitted light), so the discussion that follows applies to the parallel polarization only.

MSEF for *p*-polarized light for tri-phase system established at any point in the phase 3 is shown to depend on the incidence angle of the light at the first phase θ_1, thickness of the second layer h, and the electric field magnitude incident to the first phase at the time $t = 0$:

$$< E_{p3z}^2 > = \frac{1}{2}\left|\frac{n_1 t_{Ep} \sin\theta_1}{\tilde{n}_3}\right|^2 \exp\left[-4\pi \operatorname{Im}(\tilde{n}_3 \cos\theta_3)\frac{z-h}{\lambda}\right]\left(E_{p1}^{0t}\right)^2 \qquad (2)$$

where n_1 is the index of refraction of the IR-transparent first phase (ZnSe), $\tilde{n}_2$ and $\tilde{n}_3$ are complex refraction indices of the absorbing phases (water and platinum) and z represents the distance measured from the phase 1/phase 2 boundary. Fresnel coefficient t_{Ep} includes complex index of refraction $\tilde{n}_2$, thickness of the second layer h, wavelength of the radiation λ, as well as transmitted and reflected parts of the light in each of the phases of the stratified medium.

Because the absolute value of the electric field incident to the first layer at the time $t = 0$, E_{p1}^{0t}, in Eq. (2) is generally unknown, it is customary to express

the relative magnitude of the electric field strength. It is equal to the ratio of the MSEF established at the distance z in the direction of the propagation of the light, and that incident to the first phase, $<E_{p3z}^2>/(E_{p1}^{0t})^2$. As seen from Fig. 1, irrespective of the placement of the second and third layer in the two configurations, the metal/water boundary is always at the distance h from the boundary of the first and second layer (where h is the thickness of water or the metal layer in Otto and Kretschmann configurations, respectively).Therefore, (z-h) equals to zero, and the equation reduces to (Eq. (2a)):

$$\frac{<E_{p3z}^2>}{\left(E_{p1}^{0t}\right)^2} = \frac{1}{2}\left|\frac{n_1 t_{Ep}\sin\theta_1}{\tilde{n}_3}\right|^2 \qquad (2a)$$

The portion of the light reflected back into the phase 1 could be calculated as:

$$R_p = \left|\frac{r_{p12}r_{p23}e^{2i\beta}}{1+r_{p12}r_{p23}e^{2i\beta}}\right|^2 \qquad (3)$$

where the Fresnel coefficient r_{pjk} depend on the reflected light portions at the boundary of phases j and k, and β depends on the parameters of the second phase, $\beta = 2\pi h\tilde{n}_2\cos\theta_2/\lambda$.

Optical setup schematic

The setup for both Otto and Kretschmann configurations is essentially the same to the one described earlier.[19,25] The difference is that in the Otto configuration the IRE should be polished to mirror finish, whereas in Kretschmann configuration a metal film is deposited onto the flat side of the IRE. The best results are obtained if the IRE is an IR-transparent, high refractive index hemisphere or hemicylinder (see below). Besides the IRE, the setup includes two first--surface (*i.e.*, unprotected) gold mirrors (Fig. 2). The original focal point of the FTIR instrument's internal chamber F is raised by the first gold mirror to the point F'. If the distance d of the focal point F' from the curved surface is precisely set to be $d = r/(n_1–1)$, where r is the radius of the hemisphere and n_1 is its refractive index, the IR rays inside the hemisphere become collimated.[26] That way the angle of incidence at the working electrode/solution interface is well-defined, which is critical for this setup, as shown further.

The relative magnitude of MSEF and reflectance into the first layer at the metal/water interface for *p*-polarized IR light were calculated as a function of angle of incidence for Otto configuration for three wavelengths and the thicknesses of the water layer of 0.5 μm. The same quantities are also calculated for Kretschmann configuration, for the thickness of the metal layer of 50 nm. The wavelengths of the IR light, 3.3, 4.9 and 9.9 μm (corresponding to the wave num-

bers of 1010, 2040 and 3030 cm^{-1}, respectively) were chosen to be close to the prominent bands occurring in most spectroelectrochemical investigations, like alcohol oxidation in acidic medium. For instance, sulfate and perchlorate stretching bands of the supporting electrolyte, as well as several bands of ethanol and its partial oxidation products, acetaldehyde and acetic acid, occur around 1000–1200 cm^{-1}; linearly adsorbed carbon monoxide on most metal surfaces (CO$_L$) falls around 2000–2100 cm^{-1}; and CH$_2$ and CH$_3$ stretching modes of most organics fall around 2800–3000 cm^{-1}.[25] The results are shown in Fig. 3.
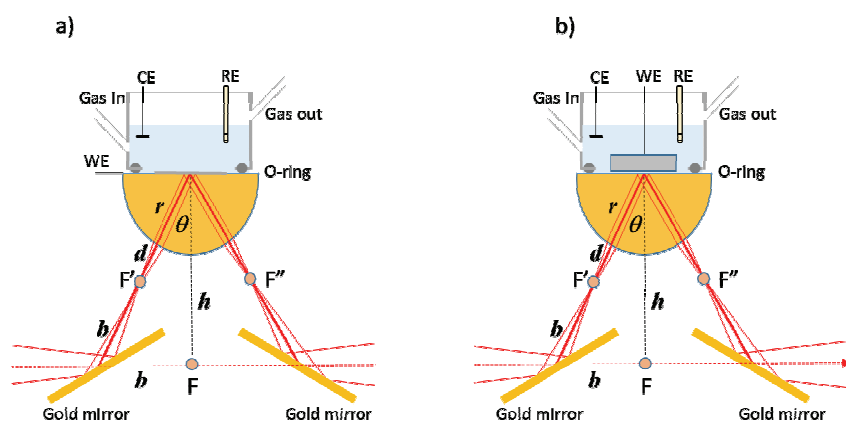

Fig. 2. Schematic representation of the attachment *for in situ* IRRAS in Kretschmann (left) and Otto configuration (right). The IR beam from a FTIR instrument is focused into the focal point F. The focal point is moved by the accessory's first folding mirror to F' in front of the curvature of the internal reflection element (IRE) hemisphere of radius r, thus collimating the light entering the hemisphere. The collimated beam strikes the IRE-electrolyte or IRE/metal interface at a precise angle of incidence θ and, upon total reflection from the interface, refocuses by the hemisphere curvature into the focal point F'' and travels further towards IR detector after the reflection of the second folding mirror. The distances are as follows: a – distance from the internal chamber wall to the folding mirror, b – distance from the folding mirror to the focal point, d – distance from the focal point to the curvature of the hemisphere, h – distance from the instrument's focal point F to the flat surface of the hemisphere.

Several important conclusions can be drawn from the plots in Fig. 3a:

i) Relative magnitude of the electric filed strength strongly depends on the wavelength of the incoming radiation. The highest magnitude of the MSEF is seen with the shortest wavelength (3.3 μm); in comparison, the maximum of the MSEF at 9.9 μm is 25 times smaller.

ii) The maxima of the MSEF peaks do not fall at the same angle of incidence, nor they coincide with the respective critical angles; the maxima of MSEF fall at 37, 35 and 40° for λ = 3.3, 4.9 and 9.9 μm, respectively, whereas critical angles for those wavelengths are 36.5, 33.1 and 30.5°, respectively.

iii) While the intensity of the MSEF peaks decreases with the increase of the wavelength of the IR radiation, no apparent trend is seen in the reflectivities.

iv) The maxima of MSEF are always higher than the critical angles, as expected.

v) The maxima of MSEF are always close to the minima of the reflectance in the first layer. That too is expected, as the incoming radiation separates into transmitted radiation that is exerted onto the phase 2/3 interface and the reflected radiation that travels back to the phase 1.
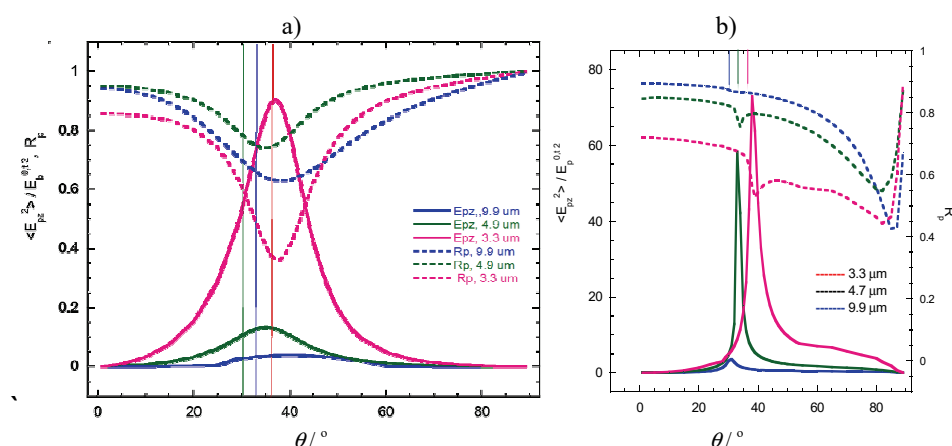

Fig. 3. Relative mean square electric field magnitude at the metal/solution interface and reflectance into the first phase (IRE) as a function of the incidence angle of the *p*-polarized IR beam onto the layer 1 in Otto (a) and Kretschmann configuration (b). The thickness of the phase 2 was set to 0.5 μm and 50 nm for the left and right plot, respectively. Vertical lines show the critical angles for three wavelengths of the IR radiation.

Conclusions similar to those above can be drawn from the MSEF in Kretschmann configuration (Fig. 3b). However, the comparison of the two plots shows some notable differences. First, the MSEF strength at the phase 2/3 interface in the Kretschmann configuration is considerably larger than that in Otto configuration; for instance, at 3.3 μm, the enhancement is about 80 times. Even larger enhancements are observed at the other two wavelengths; for 9.9 μm, the improvement in MSEF is almost three orders of magnitude. Another significant difference is that the peak of MSEF almost coincides with the critical angle, and falls in a much narrower range than that of the Otto configuration. An important consequence of the MSEF–θ plot in Kretschmann configuration is that no angle of incidence gives preferable enhancement at all wavelengths in mid IR range. For instance, as the MSEF peaks between 31 and 37°, one would expect that the average incidence angle of 34° would be the optimal compromise for the whole IR

range. However, the calculation shows that the MSEF at 3.3 μm is only about 20 % of the peak value.

Fig. 4 shows the MSEF at the phase 2/phase 3 interface and reflectivity into the phase 1 for Kretschmann configuration at $\lambda = 4.9$ μm as the function of the angle of incidence for various thicknesses of the metal layer (phase 2). Logically, as the metal layer increases in depth, the relative magnitude decreases in intensity. However, for very thin films < 10 nm) the maximum of the MSEF is slightly reduced in magnitude. From the plot, it follows that the optimal thickness of the metal layer should be less than 10 nm. The maxima of the curves coincide among themselves and occur just above the critical angle ($\theta_c \approx 33.1°$ at $\lambda = 4.9$ μm). The minima of reflectivities also coincide among themselves and fall at similar incidence angle as the maximum of the MSEFs (~34°).
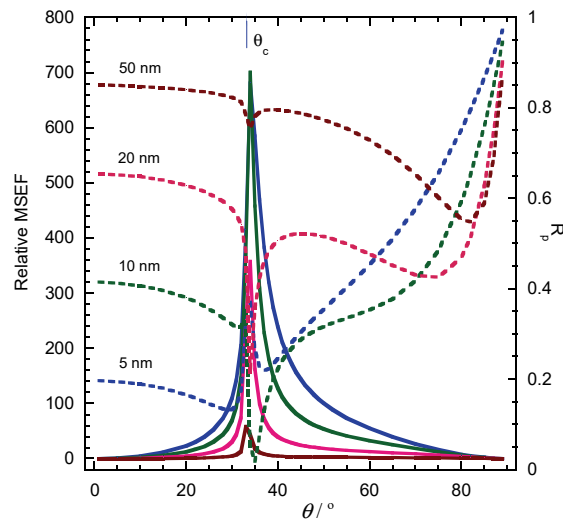

Fig. 4. Relative mean square electric field magnitude at the metal/solution interface for p-polarized light of the wavelength of 4.9 μm (2040 cm^{-1}) as a function of the angle of incidence into the first phase θ_1 for the metal thicknesses of 5, 10, 20 and 50 nm (full lines), and reflectance into the first phase (dashed lines) for ZnSe/Pt/H$_2$O tri-phase system in Kretschmann configuration.

To explore further the dependency of the MSEF on the experimentally controllable parameters (θ and h), we plotted the variation of MSEF as a function of the thickness of the metal layer for the angle of incidence of 37°, which corresponds to the optimal angle of incidence for the IR light of $\lambda = 3.3$ μm. Fig. 5 shows that the optimal thickness of the metal layer is only a few nanometers, but no metal thickness gives the highest enhancement of the MSEF for the IR light in the whole mid-IR region. Furthermore, the minima of the reflectance into the first layer do not coincide with the peak of MSEF.

From the plots presented in Figs. 3–5, it follows that MSEF for Kretschmann configuration depends strongly on both the incidence angle and the thickness of the metal layer. Unfortunately, both are difficult to control. Deposition of metals at nanometer thicknesses rarely produces a uniform layer. Osawa *et al.* have shown that thin metal layer with an average thickness of 8 nm consists of individual metal islands on top of the IRE.[27,28] Interestingly, while their plot for the reflectance of polarized light is identical to Fig. 4, their calculation for MSEF shows that it stays practically zero at all angles of incidence. We ascribe this discrepancy to the distance from the phase 1/ phase 2 boundary where the MSEF was calculated. In their case, the MSEF was calculated within the metal layer, at the half of its depth. It is logical that the MSEF must be large at the phase 2/phase 3 boundary, as the experimental confirmation found in the same work shows a considerable increase in signal-to-noise spectra in Kretschmann configuration.
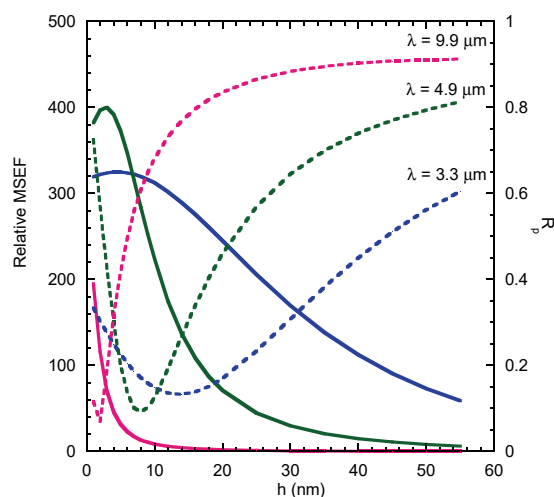

Fig. 5. Relative mean square electric field magnitude at the metal/solution interface for *p*-polarized light of the wavelength of 3.3, 4.9 and 9.9 μm (full lines) as a function of the thickness of the metal layer, and reflectance into the first phase (dashed lines) for ZnSe/Pt/H$_2$O tri-phase system in Kretschmann configuration.

On the other hand, the angle of incidence of the IR light on the first layer is difficult to control as well, especially in Kretschmann configuration where a slight maladjustment (of no more than a degree) causes the MSEF to fall considerably. Furthermore, as concluded above, no optimal angle of incidence nor thickness of the metal layer can produce adequately large enhancement in MSEF in the whole mid-IR region. Thus, one needs to select a region in which the most IR bands of interest are expected, and adjust both the thickness and the angle of incidence correspondingly. This is expensive, as it requires several IRE covered

with different thicknesses of the metal layer, and a tedious process that requires careful adjustment of the setup for every experiment.

Some discussion of similar questions of electrochemical applications of UV-Vis reflectance spectroscopy can be found in literature.[29]

CONCLUSIONS

We show that a single setup for spectroelectrochemical accessory can be used for both Otto and Kretschmann configurations that differ in the placement of the metal and solution phases. The setup involves a hemispherical internal reflection element and adjustment of the focal point of the IR light to a point before the curvature of the hemisphere. With the help of the calculation of the mean-square electric field (MSEF), we show that both angle of incidence and the thickness of phase 2 strongly influence the magnitude of MSEF. While the peaks of MSEF for different wavelengths of the IR radiation in Otto configuration are rather broad so that one particular angle of incidence can produce enhancement at all wavelengths in mid-IR region, no such enhancement is possible with the Kretshcmann configuration. However, the MSEF calculation can help in identifying the optimal thickness and angle of incidence for a particular range of IR radiation in which the peaks of interest occur. The optimized spectroelectrochemical configurations is instrumental for the identification of species in the near-surface layer and their behavior during the potential excursion.

И З В О Д
КОНФИГУРАЦИЈЕ ЗА *in situ* СПЕКТРОЕЛЕКТРОХЕМИЈСКА МЕРЕЊА У ИНФРАЦРВЕНОЈ ОБЛАСТИ

НЕБОЈША С. МАРИНКОВИЋ[1] и РАДОСЛАВ Р. АЏИЋ[2]

¹Department of Synchrotron Catalysis Consortium and Department of Chemical Engineering, Columbia University, New York, NY 10027, USA и ¹Department of Chemistry, Brookhaven National Laboratory, Upton, NY 11973, USA

Избор конфигурација за инфрацрвену (IC) спектроелектрохемију зависи од типа испитиване реакције. Најчешће коришћен систем је Ото (Otto) кофигурација у коме се електролит стисне између електроде и елемента унутрашње рефлексије (IRE). Међутим, други систем са електродом у облику филма депонованог на равну страну IRE (Кречман (Kretschmann) конфигурација) добија на популарности, не само због повећања осетљивости већ и зато што омогућује испитивања електрохемијских реакција при којим се издваја гас. Коришћењем Френелових (Fresnel) једначина за трофазне слојеве показали смо да је јачина електричног поља на додиру фаза метал–раствор, а тиме и количина енергије пренешена на адсорбоване честице у Ото конфигурацији, прилично флексибилна у избору оптималног упадног угла IC зрачења и дебљине слоја воде. Насупрот томе, Кречман конфигурација је врло осетљива на параметре оптичког система, тако да су изчаравања јачине електричног поља потребна како би се пронашли оптималан упадан угао и дебљина металног слоја који дају максимално појачање у средњем IC подручју где се појављују траке које нас интересују.

REFERENCES

1. P. R. Griffiths and J. A. de Haseth, *Fourier Transform Infrared Spectrometry*, 2nd ed., J. Wiley, New York, 2007 (ISBN-13: 978-0471194040)
2. F. M. Mirabella, *Internal Reflection Spectroscopy: Theory and Applications*, Marcel Dekker, New York, 1993
3. N. J. Harrick *Internal Reflection Spectroscopy*, Interscience Publishers, J. Wiley and Sons, New York, 1967
4. R. G. Greenler, *J. Chem. Phys*. **44**(1966) 310 (https://doi.org/10.1063/1.1726462)
5. R. G. Greenler, *J. Chem. Phys.* **50** (1969) 1963 (https://doi.org/10.1063/1.1671315)
6. R. G. Greenler, *J. Vac. Sci. Technol.* **12** (1975) 1410 (https://doi.org/10.1116/1.568552)
7. A. Bewick, K. Kunimatsu, B. S. Pons, J. W. Russell, *J. Electroanal. Chem.* **160** (1984) 47 (https://doi.org/10.1016/S0022-0728(84)80114-X)
8. A. Antonio Berna, A. Rodes, J. M. Feliu, in In-situ *Spectroscopic Studies of Adsorption at the Electrode and Electrocatalysis*, S.-G. Sun, P. A. Christensen, A. Wieckowski, Eds., Elsevier, Amsterdam, 2007, pp. 1–32
9. J.-M. Leger, F. Hahn, in In-situ *Spectroscopic Studies of Adsorption at the Electrode and Electrocatalysis,* S.-G. Sun, P. A. Christensen, A. Wieckowski, Eds., Elsevier, Amsterdam, 2007, pp. 63–98
10. C. Korzeniewski, in *Single-crystal Electrochemistry and Electrocatalysis* In-situ *Spectroscopic Studies of Adsorption at the Electrode and Electrocatalysis*, S.-G. Sun, P.A. Christensen, A. Wieckowski, Eds., Elsevier, Amsterdam, 2007, pp. 179–208
11. A. Otto, *Phys. Stat. Sol.* **26** (1968) K99 (https://doi.org/10.1002/pssb.19680260246)
12. P. W. Faguy and N.S. Marinkovic, *Appl. Spectrosc.* **50** (1996) 394 (https://doi.org/10.1366/0003702963906302)
13. M. Li, N. Marinkovic, in *Infrared Spectroscopy: Theory, Developments and Applications*, D. Cozzolino, Ed., Nova Science Publishers, New York, Ch. 14, pp. 307–332 (ISBN: 978-1-62948-521-8)
14. J. W. Russel, J. Overend, K. Scanlon, M. Severson, A. Bewick, *J. Phys. Chem.* **86** (1982) 3066 (https://doi.org/10.1021/j100213a005)
15. S. Pons, *J. Electroanal. Chem.* **150** (1983) 495 (https://doi.org/10.1016/S0022-0728(83)80229-0)
16. D. S. Corrigan, L. W. H. Leung, M.J. Weaver, *Anal. Chem.* **59** (1987) 2252 (https://doi.org/10.1021/ac00145a009)
17. H. Seki, K. Kunimatsu, W. G. Golden, *Appl. Spectrosc.* **39** (1985) 437 (https://doi.org/10.1366/0003702854248593)
18. E. Kretschmann, H. Reather, *Z. Naturf.* **23** (1968) 2135 (https://doi.org/10.1515/zna-1968-1247)
19. N. Marinkovic, *Zaštita Materijala* **59** (2018) 273 (10.5937/ZasMat1802273M)
20. P. W. Hansen, *J. Opt. Soc. Am.* **58** (1968) 380 (https://doi.org/10.1364/JOSA.58.000380)
21. P. W. Hansen, in *Advances in Electrochemistry and Electrochemical Engineering,* Vol. 9, P. Delahay, C. W. Tobias, Eds., John Wiley and Sons, New York, 1973, pp.1–60
22. On-line program Wolfram Alpha, www.wolframalpha.com (accessed 8/16/19)
23. Refractive indices for ZnSe, water and Pt are given at https://refractiveindex.info/?shelf=main&book=ZnSe&page=Querry, http://refractiveindex.info/?shelf=main&book=H2O&page=Hale https://refractiveindex.info/?shelf=main&book=Pt&page=Windt(accessed 8/16/19)
24. Permeability in Wikipedia, https://en.wikipedia.org/wiki/Permeability_(electromagnetism) (accessed 8/16/19)

25. N. Marinkovic, M. Li and R. R. Adzic, *Top. Curr. Chem.* **377** (2019) 11 (http://link.springer.com/10.1007/s41061-019-0236-5)
26. See Lensmaker's equation, for plano-convex lens ($R_2 = \infty$ and $d = 0$), https://en.wikipedia.org/wiki/Lens#CITEREFHecht1987 (accessed 8/16/19)
27. M. Osawa, M. Kuramitsu, A. Hatta, W. Suetaka, *Surf. Sci.* **175** (1986) L787 (https://doi.org/10.1016/0039-6028(86)90001-4)
28. M. Osawa in *Advances in Electrochemical Science and Engineering. Diffraction and Spectroscopic Methods in Electrochemistry*, Vol. 9, R. C. Alkire, D. M. Kolb, J. Lipkowski, P. N. Ross, Eds., Wiley-VCH, Berlin, 2009, pp. 269–314 (ISBN-13: 9783527313174)
29. R. R. Adzic, *J. Serb. Chem. Soc.* (ex. *Bulletin de la Societe Chimique, (Beograd)*) **39** (1974) 661 (in Serbian).